Exploration of a rich variety of breather modes in Josephson ladders

P. Binder and A. V. Ustinov*

Physikalisches Institut III, Universität Erlangen-Nürnberg, Erwin-Rommel-Straße 1, D-91058 Erlangen, Germany
(Received 22 March 2002; published 19 July 2002)

We report on systematic measurements of localized rotational modes in Josephson junction arrays. These modes, also known as rotobreathers, persist under the action of uniform bias force. In contrast to previous experiments, here we focus on systems with *strong coupling* between rotators. In ladders with either open or periodic boundary conditions, we observe a very rich variety of stable dynamic states including symmetric, asymmetric, combined, hybrid, coupled, and truncated modes. The switching scenarios between different states are discussed in detail.

PACS number(s): 05.45.Yv, 63.20.Ry, 74.50.+r

I. INTRODUCTION

Rotational and oscillatory excitations in discrete nonlinear lattices that are spatially localized on the scale comparable to the lattice constant have gained much interest in past few years [1–3]. These excitations have been named as intrinsically localized modes or *discrete breathers*. They are believed to be as generic for discrete nonlinear lattices as solitons are for continuous nonlinear media. Discrete breathers play an important role in the dynamics of various physical systems consisting of coupled nonlinear oscillators. There have been recent experiments that reported on generation and detection of discrete breathers in diverse systems such as low-dimensional crystals [4], antiferromagnetic materials [5], coupled optical waveguides [6], and Josephson junction arrays [7–10].

A biased Josephson junction behaves very similar to its mechanical analog that is a forced and damped pendulum. An electric bias current flowing across the junction is analogous to a torque applied to the pendulum. The maximum torque that the pendulum can sustain and remain static corresponds to the critical current I_c of the junction. For low damping and bias below I_c, the junction allows for two states: the superconducting (static) state and the resistive (rotating) state. The phase difference φ of the macroscopic wave functions of the superconducting islands on both sides of the junction plays the role of an angle coordinate of the pendulum. According to the Josephson relation, a junction in a rotating state generates dc voltage $V = (1/2\pi)\Phi_0\langle d\varphi/dt\rangle$, where $\langle\cdots\rangle$ is the time average. By connecting many Josephson junctions by superconducting leads, one gets an array of coupled nonlinear oscillators.

In this paper we present results of systematic search for localized rotational modes (rotobreathers) in Josephson ladders. Rotobreathers are 2π-periodic solutions in time that are exponentially localized in space [11,12]. In contrast to the previously reported experiments [7–10], we study Josephson ladders in the *strong coupling limit*. We undertake an extensive measurement expedition to search for all possible complex states in ladders. A rich variety of rotobreathers that all

persist under the action of the spatially uniform force is catched as reported below.

We investigated ladders consisting of Nb/Al-AlO$_x$/Nb underdamped Josephson tunnel junctions [13]. Each cell of the ladder contains four small Josephson junctions. We studied the ten-cell ladders with either open or periodic boundary conditions. The ladder geometry is schematically shown in Fig. 1. As usual, we define *vertical* junctions (JJ_V) as those in the direction of the external bias current and *horizontal* junctions (JJ_H) as those transverse to the bias. The ladder voltage was read across the central vertical junction. The damping coefficient $\alpha = \sqrt{\Phi_0/(2\pi I_c C R_{sg}^2)}$ is the same for all junctions as their capacitance C and subgap resistance R_{sg} scale with the area and $C_H/C_V = R_{sgV}/R_{sgH}$. The damping α in the experiment can be controlled by temperature and its typical values varies between 0.1 and 0.02. There are two types of couplings between cells in a ladder. The first is the inductive coupling between the cells that is expressed by the self-inductance parameter $\beta_L = 2\pi L I_{cV}/\Phi_0$, where L is the self-inductance of the elementary cell. The second is the nonlinear Josephson coupling via horizontal junctions. The ratio of the horizontal and vertical junction areas is called the
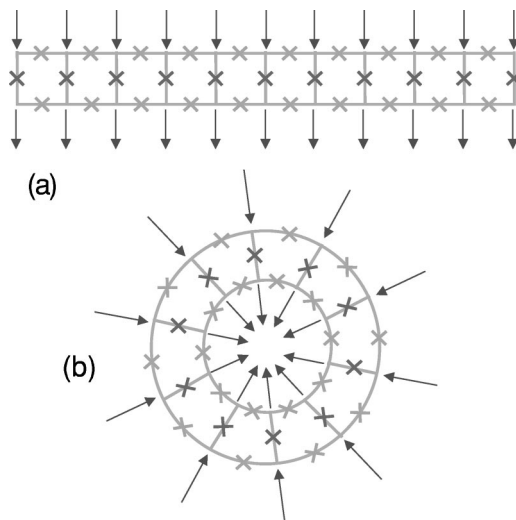
FIG. 1. Schematic view of a linear ladder (a) and an annular ladder (b). Arrows indicate the direction of the externally applied bias current.

*Electronic address: ustinov@physik.uni-erlangen.de; URL: http://www.physik.uni-erlangen.de/pi3/ustinov

66 016603-1

anisotropy factor and can be expressed in terms of the junction critical currents $\eta = I_{cH}/I_{cV}$. If $\eta = 0$, the vertical junctions are decoupled and operate independently from one another. That corresponds to the so called anticontinuous limit. On the other hand, if $\eta = \infty$ the ladder behaves like a parallel one-dimensional array. Rotobreathers do not exist in this limit since no magnetic flux can enter the array through the horizontal junctions.

Since the nonlinear localized modes cease to exist in the continuum case, it is interesting to increase the anisotropy η to the largest possible values at which these modes may still occur. In this work we observe rotobreathers in Josephson ladders with the highest anisotropy factors ($\eta = 0.73$ and $\eta = 1.0$) studied up to now.

To relate the roles played by the parameters mentioned above, we briefly quote the equations of motion for our system (see Ref. [12] for details):

$$\ddot{\varphi}_l^V + \alpha \dot{\varphi}_l^V + \sin \varphi_l^V = \gamma + \frac{1}{\beta_L}(\Delta \varphi_l^V - \nabla \widetilde{\varphi}_{l-1}^H + \nabla \varphi_{l-1}^H),$$

$$\ddot{\varphi}_l^H + \alpha \dot{\varphi}_l^H + \sin \varphi_l^H = -\frac{1}{\eta \beta_L}(\varphi_l^H - \widetilde{\varphi}_l^H + \nabla \varphi_l^V), \qquad (1)$$

$$\ddot{\widetilde{\varphi}}_l^H + \alpha \dot{\widetilde{\varphi}}_l^H + \sin \widetilde{\varphi}_l^H = \frac{1}{\eta \beta_L}(\varphi_l^H - \widetilde{\varphi}_l^H + \nabla \varphi_l^V),$$

where $\varphi_l^V, \varphi_l^H, \widetilde{\varphi}_l^H$ are the phase differences across the lth vertical junction and its right upper and lower horizontal neighbors, $\nabla \varphi_l = \varphi_{l+1} - \varphi_l$, $\Delta \varphi_l = \varphi_{l+1} + \varphi_{l-1} - 2\varphi_l$, and $\gamma = I_B/I_{cV}$ is the normalized bias current.

In order to generate discrete breathers in a ladder we used the technique described in Ref. [8]. Two extra bias leads were attached to one of the vertical Josephson junctions (we call it the middle junction) to apply a local current $I_{local} > I_{cV}$. This current switches the vertical junction in the resistive state. At the same time, being forced by magnetic flux conservation, horizontal junctions on both sides of the vertical junctions also switch to the resistive state. After that I_{local} is reduced and, simultaneously, the uniform bias I_B is tuned up. In the final state, we keep the bias I_B smaller than I_{cV} and have reduced I_{local} to *zero*. By changing the starting value of I_{local} it becomes possible to get more than one vertical junction rotating. The experience showed that better results are obtained by reducing first I_{local} a bit and then starting with the increase of I_B. Also the final value of the uniform bias I_B is important: the smaller the rotobreather, the higher the final value should be chosen. When trying the slightly different current sweep sequence described in Ref. [7] we generated mainly states with many rotating vertical junctions.

In all measurements presented below, we have detected the dc voltage across the middle vertical junction as a function of the bias current I_B that was uniformly applied to the whole ladder. We used the method of low temperature scanning laser microscopy [14] to obtain images from the dynamic states of the ladder. In this method, a laser beam locally heats the sample, which changes the dissipation in an area of several micrometers in diameter. If the junction at the

FIG. 2. Classification of rotobreather states.

heated spot is in the resistive state, a voltage change corresponding to a small decrease of the rotator frequency is measured. For junctions in the superconducting state no response is expected. By scanning the laser beam over the whole ladder we can visualize the rotating oscillators. The measured ladder states are shown then as two-dimensional (2D) gray scale maps. The x-y coordinates are the coordinates in the sample plane and the gray scale reflects the measured voltage response during the laser scanning.

II. CLASSIFICATION OF ROTOBREATHERS

We use a special classification for the different rotobreather modes found in our measurements. This classification helps to guide the reader through the breather variety described below. It makes it easier describing similarities and distinctions between various modes found. The definition of observed types of rotobreathers is presented in Fig. 2. Here the large and small circles indicate whirling vertical and horizontal junctions, respectively. These modes distinguish from one another through the number of whirling horizontal junctions at their edges and interior. For every type of breathers we observed similar states of single site, two sites, three sites, and so on. The number of sites is defined as the number of rotating vertical junctions.

The first type is the *symmetric* breather. This state has both up-down symmetry and left-right symmetry. On each end of the whirling vertical junctions there are also two adjacent horizontal whirling junctions. Another common type is the so called *asymmetric* breather. This notation indicates that this state has lower symmetry than the symmetric mode. Still, the asymmetric state obeys the left-right mirror symmetry. At this mode either the upper or the lower horizontal junctions, which are adjacent to the whirling vertical ones, rotate. The *combined symmetric* breather is invariant under an up-down mirror reflection followed by a left-right mirror reflection. This mode has similar I-V characteristics to that of the asymmetric breather because of the same number of rotating horizontal and vertical junctions. For another mode two horizontal junctions on one side and only one horizontal junction on the other side rotate. This state shows no symmetry and we

call it *hybrid* breather. Any of the above mentioned types of discrete breathers can couple together and form *coupled* or *combined* breathers. There are at least two groups of whirling vertical junctions in coupled breathers, which differ by their rotation frequencies. Finally, all the above mentioned types of discrete breathers are pure states deep inside a ladder. If the ladder has open boundaries and the breather touches one of them, there are no horizontal junctions to whirl on the breather side. We call this state as a *truncated* breather.

It has to be noted that the above classification is introduced irrespective of any detail of the internal dynamics of the breathers, i.e., temporal periodicity of rotation for different sites, mutual phase shifts, etc. The used measurement technique does not provide information about the temporal dynamics of junctions that is of picosecond scale. We only measure the Josephson voltage on the junctions that is proportional to their mean rotation frequency of the order of several 100 GHz.

III. LINEAR LADDER WITH OPEN BOUNDARIES

In this section we present measurements of a linear Josephson junction ladder with the highest anisotropy factor ($\eta=1.0$) studied experimentally up to now. The higher the anisotropy factor the more difficult is the observation of localized modes, but still it turned possible to observe quite a few of them. This isotropic ladder has ten cells as shown in Fig. 1(a). The cells' size amounts to 24 μm and it is mainly filled by the wide superconducting electrodes. The size of the hole of the cell is only about 3×3 μm^2. The measurements were conducted at a temperature of 5.3 K. The critical current per Josephson junction at this temperature was 59 μA and the self-inductance parameter β_L amounts to 2.3. The biasing was done through on-chip resistors of 32Ω each. The local current for the creation of the breather was injected in the central vertical Josephson junction. We show here the measured laser scanning voltage response images and then describe the observed current-voltage (I-V) characteristics.

A. Laser scanning images

Some of the states observed in the isotropic ladder are shown in Fig. 3. The diagonal of the maximum scanning area was just big enough to fit the whole ladder, therefore the images are aligned along the diagonal of the plot. First, the homogeneous whirling mode is presented in Fig. 3(a). All other pictures shown in this figure are truncated breathers or, in other words, breathers in which one end is extended up to the border of the ladder. We did not observe smaller truncated breathers than the ones with six vertical junctions in the resistive state. The obvious explanation is that for creating the rotobreather we drove initially the middle (sixth) vertical junction into resistive state. Figures 3(b)–3(f) show all the possible truncated symmetric breathers in this system. In Fig. 3(f) only the left, marginal vertical junction is in the superconducting state aside with many horizontal junctions.

The only asymmetric truncated mode that we found is presented in Fig. 3(g). The following Figs. 3(h)–3(k) are truncated asymmetric breathers coupled with a single-site
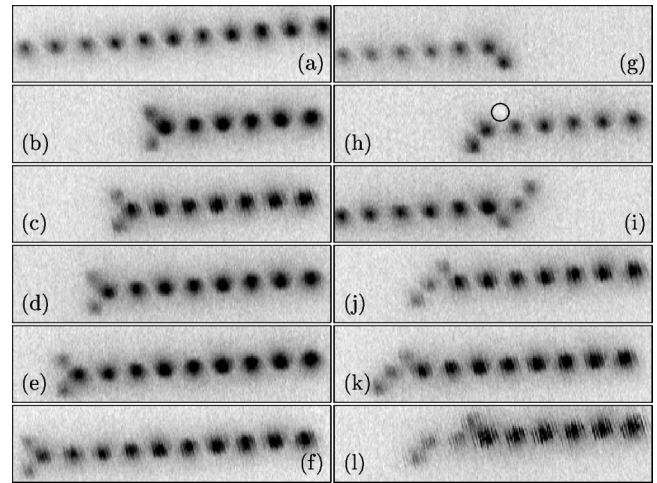
FIG. 3. The homogeneous whirling mode (a) and several truncated rotobreathers (b)–(l) in an isotropic ladder.

breather. Note that one of the whirling horizontal junctions in Fig. 3(h) shows an inverted (white) response. Here, the voltage V of the vertical junction of the single-site part of the state (the middle vertical junction) was used for the measurement with the scanning laser microscope. This voltage is smaller than that of the adjacent right vertical junction, in opposite to the other cases. Hence an increase of the voltage of the horizontal junction due to extra damping induced by the laser spot leads to a *decrease* of the measured voltage, which appears on the image as the white response. This state is identical to those in Figs. 3(i)–3(k) apart from the number of whirling vertical junctions. It is remarkable that the voltage of the vertical junction, which forms the single-site breather is fixed for a given voltage of the vertical junctions from the main body of the coupled state. We were able to create and measure every state several times without observing any change in the voltages for a given bias point.

Figure 3(l) shows a truncated six-site breather coupled to a two-site breather with top and bottom whirling horizontal junctions. Also here, the whirling vertical junctions in the two parts of the mode have different voltages. Coupled states where both parts are multisite breathers are very rare but still exist.

A few compact localized modes are presented in Fig. 4. In the Figs. 4(a)–4(c) the single-, three-, and four-site asym-
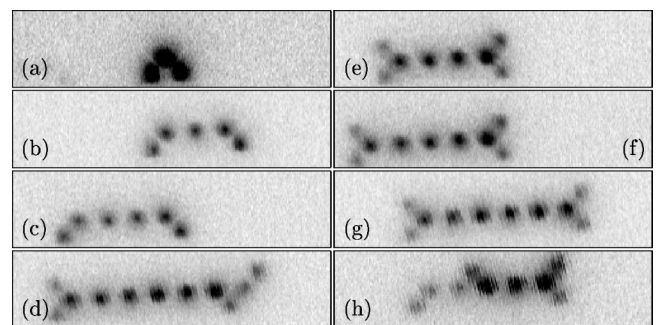
FIG. 4. Asymmetric (a)–(c), symmetric (e)–(g), and coupled (d) and (h) localized modes.
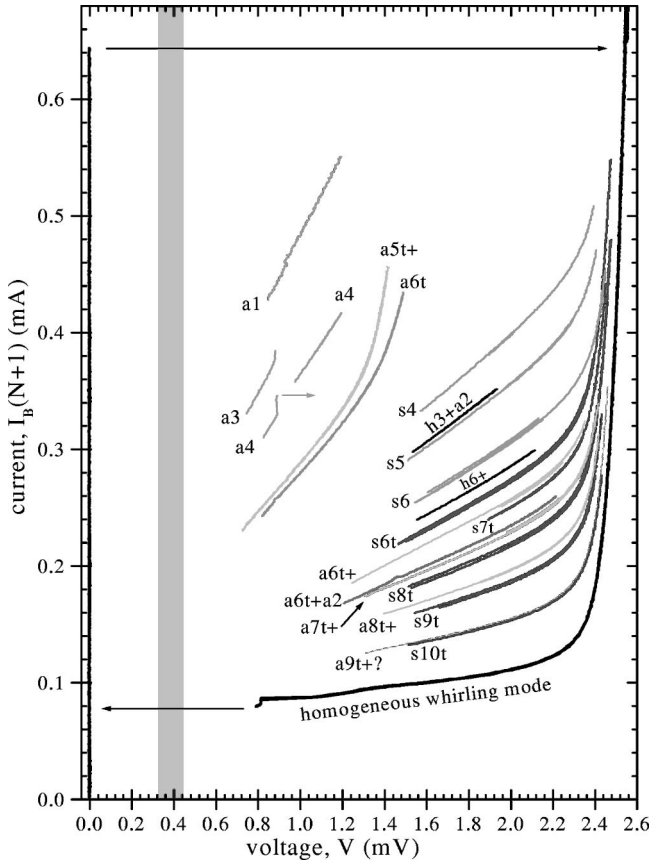
FIG. 5. The I-V map of an isotropic ladder. Many different localized modes are shown. The gray region indicates the frequency range of the upper plasmon band.

metric breathers are seen, respectively. Several symmetric breathers are shown in Figs. 4(e)–4(g). It turned impossible to observe any smaller symmetric rotobreathers than the four-site mode in Fig. 4(e). Here, the voltages of the upper and lower horizontal junctions have the same value aside from the sign. The remaining two Figs. 4(d) and 4(h) display two different coupled states. Figure 4(d) shows a six-site hybrid breather coupled to a single-site one. Figure 4(h) is an exceptionally spectacular state. We observe here two coupled multisite rotobreathers, namely, a three-site hybrid coupled with a two-site breather.

B. Current-voltage characteristics

The complete set of I-V characteristics for this isotropic Josephson junction ladder looks very crowded with all the curves of the observed localized modes. All measured curves are shown in Fig. 5. Every curve in this rich family corresponds to a particular dynamic state of the ladder, which remains stable along the curve. The very left vertical line denotes the superconducting state and the very bottom right curve is the uniform whirling mode of the ladder. The three upper characteristics indicated as $s4$, $s5$, and $s6$ are symmetric four-site, five-site, and six-site breathers, respectively. These curves start just above the bias point I_B where the horizontal junctions reach their retrapping current. The voltage V at this end of the curve is about 1.55 mV, which is

around the double of the lowest voltage of the homogeneous whirling mode. The curves end up at a relatively high bias point where the bending due to the gap is already well visible.

The spectacular mode that is a combination of a three-site hybrid and a two-site asymmetric [with whirling top and bottom horizontal junction, cf. Fig. 4(h)] breather denoted as $h3+a2$ lies just above the $s5$ mode. The next line below the $s6$ mode indicated as $h6+$ is another coupled mode: a six-site hybrid plus a single-site breather (c.f. Fig. 4(d)). Further, the truncated six-site to ten-site symmetric breathers are marked in Fig. 5 as $s6t$ to $s10t$. They cease to exist at the same minimum voltage as the pure symmetric ones. The exception is the $s7t$ mode for which we were able to trace only the upper part of the curve. In the same region we find also the truncated six-site to eight-site asymmetric breathers coupled with a single-site one, which are indicated as $a6t+$ to $a8t+$, respectively. We did not take any electrical image from the characteristic denoted as $a9t+?$ but we believe that it belongs also to the same group. The characteristic of the last coupled state in this region which is shown in Fig. 3(l) is denoted as $a6t+a2$. Actually, this mode is located on the I-V plane in that region where also the bigger symmetric breathers ($s7-s10$) are expected. The stability range in the parameter space looks smaller for these breathers in comparison with the truncated ones and this may be the reason why we did not observe them.

There is also another characteristic ($a5t+$) that belongs to the family of the truncated asymmetric breathers bounded with a single-site one. It is found in the central upper part of the I-V plane. The main body of this state has five whirling vertical junctions. But the voltage V is always measured at the sixth middle vertical junction that is the whirling junction of the single-site part of this coupled mode. As we can see in Fig. 5, its voltage is lower than that of the main whirling body. When this voltage approaches $V \approx 0.75$ mV the retrapping current is reached where both the single-site part and the whole state ceases to exist. The minimum voltage of the $a6t+-a9t+$ curves lies between the typical voltages where the retrapping current for asymmetric and symmetric breathers is reached.

The voltage V_V^{main} of the vertical junction in the main body of a combined breather is $V_V^{main}=V_H^{margin}+V_H^{body}$ with V_H^{margin} being the voltage of the marginal horizontal junction and V_H^{body} the voltage of the horizontal junction between main body and single-site part. The curves in Fig. 5 show that at low bias current the horizontal junction, which is surrounded by whirling vertical junctions, is strongly driven by them. It still remains whirling although the voltage drops well below 0.75 mV, the voltage where the retrapping current is reached.

The last three curves at the left upper part of Fig. 5 are asymmetric breathers. Counted from the top they are the characteristics of single-site ($a1$), three-site ($a3$), and four-site ($a4$) asymmetric breathers. The last one consists of two parts. In the lower part we observe a pronounced resonance (state of nearly constant voltage, i.e., constant frequency) that shows a small back bending. By increasing the bias cur-

rent during the measurement a jump occurred from the top of the resonance to the homogeneous whirling state. Independently, it was possible to trace a part of the upper characteristic of this state. Another resonance can be seen at a slightly lower voltage at the top of the characteristic of the $a3$ mode. Its voltage correspond very well to the double of the upper frequency of the plasmon band. This band is shown in Fig. 5 as a gray region for $\gamma=0.51$. This upper limit of the bounded dispersion relation also depends slightly on the bias current.

The switching behavior between different modes does not make the observation of rotobreathers easy in this isotropic ladder. A jump to the whirling mode occurred almost always from the upper end of all localized modes. That is always true for the asymmetric breathers. From the bottom of the characteristics of the symmetric and the truncated breathers a switching to the homogeneous whirling mode could almost always be observed. From bottom end of the curves corresponding to the pure asymmetric breathers a jump to the superconducting state occurred.

IV. ANNULAR LADDER WITH PERIODIC BOUNDARY CONDITIONS

In this section measurements of an annular ladder are presented [15]. This system is described by the ladder equations (1) with periodic boundary conditions. Figure 1(b) shows a schematic view of this ladder. The bias current is applied uniformly in each outer node and extracted from each inner node. For one of the vertical junction there are extra bias leads for the injection of the local current (not shown). Due to the periodic boundary conditions, the number of types of breathers, which can be found is less than in linear ladders with open boundaries. Obviously, no truncated discrete breathers can be expected for the annular case. Few other sophisticated discrete breathers found in the linear ladders are also forbidden in annular ladders. The reason is that the magnetic flux cannot be accumulated in the interior of the ladder, i.e., the sum of voltages on inner horizontal junctions should be zero.

Because of the small diameter of the ten-cell annular ladder, we had to put all the thin film resistors, which bias the inner nodes, outside the ring. The superconducting connections between the bias resistors and the inner node are laid above the vertical Josephson junctions. Inside the ladder there is only a small resistor ($R=4\,\Omega$). Interrupting the superconducting bias leads to each node by this resistance is supposed to facilitate free motion of magnetic flux in the ladder. The annular ladder has an outer diameter of 140 μm. The size of the cell hole amounts to 5×5 μm^2. The distance between the vertical Josephson junctions is 29 μm. The ladder ring has an anisotropy $\eta=0.73$ and the self-inductance parameter $\beta_L=1.5$ at $T=5.8$ K. The critical current of the vertical junctions $I_{c\,V}$ was 37 μA.

A. Transitions between breather states

Before the complete set of I-V characteristics of the annular ladder is discussed, let us focus on a few particular I-V traces, which are relevant for understanding of the transitions between breather states. All states were created in a
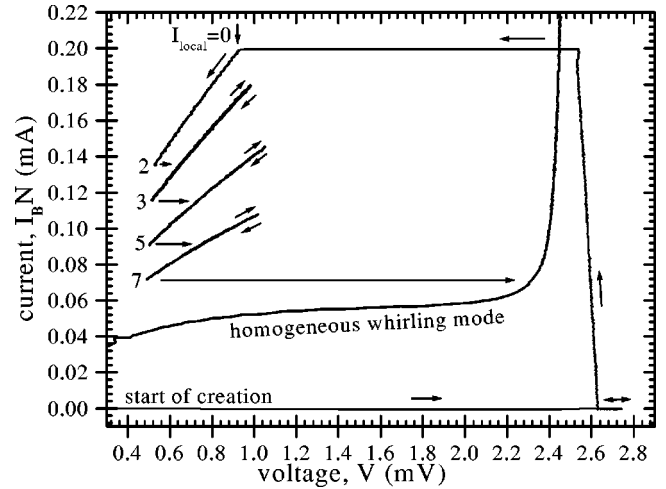
FIG. 6. The I-V curve of an annular ladder with traces used for the generating process of a rotobreather. The curves correspond to symmetric breathers and the numbers indicate the number of whirling vertical junctions.

computer-controlled way. The voltage V is measured at the Josephson junction with the local bias leads, which is used for creation of the rotobreathers.

The total bias current I_BN dependence versus the local voltage V is shown in Fig. 6. In this plot the I_B-V characteristics with $I_{local}\neq0$ during the breathers' creation process is also indicated. First, the horizontal trace with $I_B=0$ is done until the voltage appears. Second, the nearly vertical part with approximately $I_B+I_{local}=$const is traced, where the bias current I_B and the local current I_{local} are simultaneously increased and decreased, respectively. The slight deviation from $V=$const in this part of the computer-controlled sweep is due to a current redistribution over the neighboring cells through the adjacent horizontal junctions. In the last part the local current I_{local} is decreased to zero. At the end of this trace (the left end of the upper horizontal I-V line), $I_{local}=0$ and we observe a symmetric two-site breather supported by the uniform bias current I_B. From this point several transitions between different breather states are observed by changing the bias current I_B.

Each breather in Fig. 6 is found to be stable along its particular branch. On a given branch the damping of the junctions in the rotating state is compensated by the driving force of the bias current I_B. The transitions between the branches are discontinuous in voltage. The measurements shown in Fig. 6 demonstrate that the transition occurs when the retrapping current of one of the horizontal junctions is reached. Here we find mainly jumps to a higher voltage branch, typically a multisite breather with more vertical junctions whirling than in the initial state. Sometimes the transition goes directly to the homogeneous whirling mode, which is also plotted in Fig. 6. In this figure we see transitions from a two-site breather to a three-site breather, then to a five-site breather, a seven-site breather, and finally to the homogeneous whirling mode.

There exists also another transition process shown in Fig. 7. It is similar to that observed in the linear ladders, but this type of transition is more rare in annular ladders. Figure 7
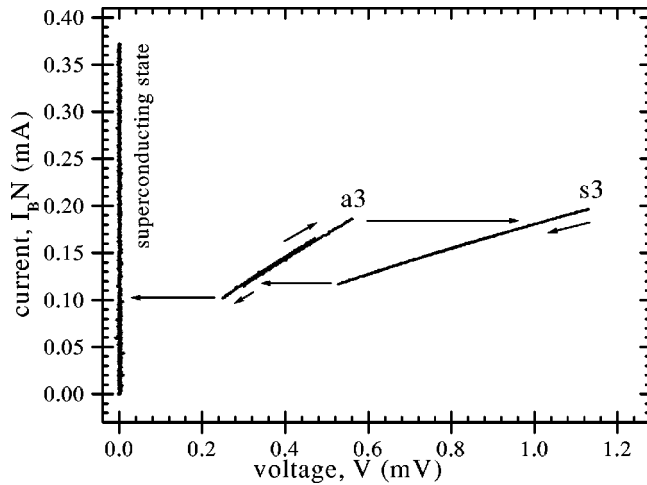
FIG. 7. Hysteretic transitions between an asymmetric three-site breather and a symmetric three-site breather.

shows the transition between the symmetric three-site breather ($s3$) and the asymmetric three-site breather ($a3$). By further decreasing the bias current a transition to the superconducting state occurs when the retrapping current of the vertical junction is reached. Increase of the bias current along the resistive branch $a3$ leads to a transition back to $s3$ state or, even more often, to a bigger multisite state.

B. Laser-scanning images

We obtained many laser-scanning voltage images of the annular ladder showing a big variety of different localized excitations. All pictures are arranged in the way that the Josephson junction with the local current injection leads is the one at the very top.

The homogeneous whirling state with all vertical junctions in the resistive state is shown in Fig. 8(a). The straight radial lines on the top of the round spots, which are the Josephson junctions, indicate the bias leads to the inner
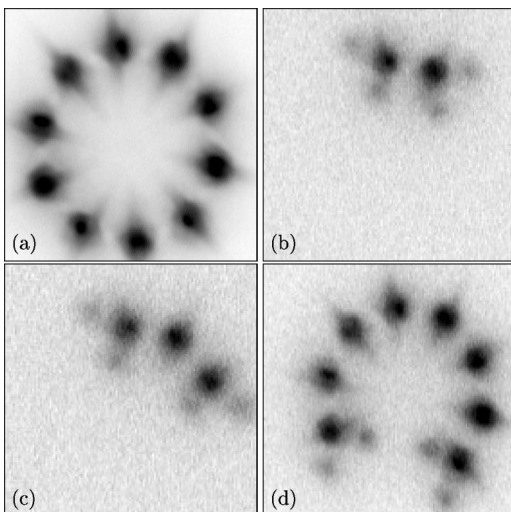
FIG. 8. Voltage images of the homogeneous whirling mode (a) and of two-site (b), three-site (c), and eight-site (d) symmetric rotobreathers.
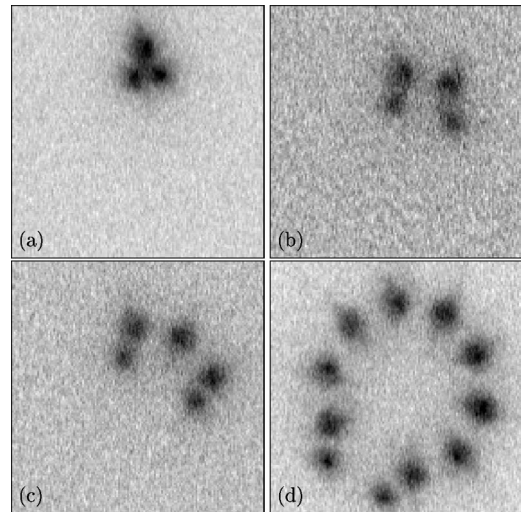
FIG. 9. Voltage images of single-site (a), two-site (b), three-site (c), and nine-site (d) asymmetric rotobreathers.

nodes. Because of their good thermal conductivity the heating of these leads also implies a heating of the junction, which gives a discernible response.

Some of the observed symmetric breathers are shown in Figs. 8(b)–8(d). In Fig. 8(b) a two-site breather and in Fig. 8(c) a three-site breather can be seen. Around the vertical junctions two horizontal junctions on every side are whirling. Because of the small diameter of the annular ladder the breather looks strongly bent. The symmetric breathers were very stable and it was possible to take all their images starting from the two-site and up to the eight-site breather. The latter one is presented in Fig. 8(d). We were able to trace only a small piece of the I-V characteristic of the nine-site breather (see following section). No track was observed for the single-site breather. Perhaps it was only matter of luck, as there is no obvious reason why a symmetric single-site breather should not exist in this ladder. In these measurements the voltage of the horizontal junction was always half of the voltage of the vertical junctions.

Several examples of asymmetric breathers are shown in Fig. 9. There are a single-site, a two-site, a three-site, and a nine-site breather in Figs. 9(a)–9(d), respectively. It was also possible to obtain images of all the other asymmetric multisite breather states. The inner horizontal junctions were whirling in most cases as in Figs. 9(a)–9(c), but sometimes also the outer horizontal junctions were excited as in Fig. 9(d). A possible reason for this different occurrence can be the annular geometry of the sample. There may be expected a circulating current through the inner horizontal junctions due to magnetic flux trapped in the ring, which facilitates to their switching to the whirling mode.

Another not yet shown type of rotobreathers is illustrated in Fig. 10. On one side of the breather the upper and the lower horizontal junctions are whirling, as it is usually the case for a symmetric breather. But on another side the last vertical junction is whirling with a smaller frequency as indicated by a lighter voltage response. This is possible because just beside this vertical junction, so to speak in the interior of the localized mode, one horizontal junction is
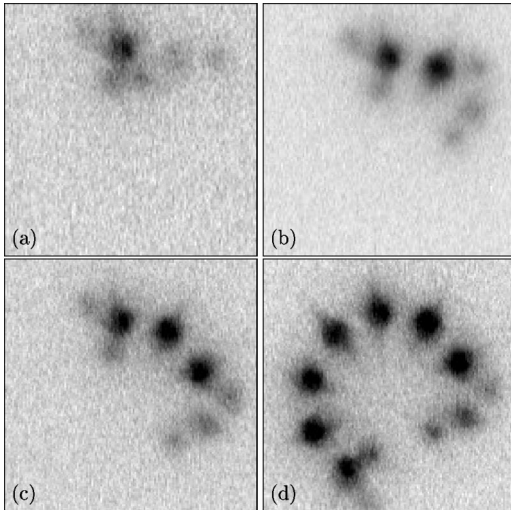
FIG. 10. Electrical images of a single-site (a), two-site (b), three-site (c), and seven-site (d) hybrid breather coupled with a single-site breather.

whirling as well. At the very boundary of the breather another horizontal junction is whirling, as it is usual for an asymmetric breather. To fulfill the magnetic flux conservation the outer horizontal Josephson junctions must have the same voltage. The same is true for the inner horizontal junctions. It is not mandatory, however, that the inner and outer horizontal junctions have the same voltage. Actually, the response detected for the rotobreather that is shown in Fig. 10(d) indicates different voltages for the outer and inner horizontal junctions. In Figs. 10(a)–10(d), we have one-site, two-site, three-site, and seven-site hybrid breathers, respectively, each of them coupled to a single-site breather. It was possible to take electrical images of all but the eight-site hybrid breather coupled to a one-site breather. We never observed the coupled state of two multisite breathers in this ladder.

C. Current-voltage characteristics

The full I-V map of the annular ladder is a combination of many I-V traces such as those shown in Figs. 6 and 7. Figure 11 shows all the different states observed during many measurements. Only the part of the I-V curve with $I_{local}=0$ is presented. Because of small changes in the temperature during one helium refill cycle of the optical cryostat there are small shifts in the characteristics for some localized modes. The vertical line on the left side corresponds to the superconducting (static) state. The rightmost bottom curve accounts for the spatially homogeneous whirling state (all vertical junctions rotate synchronously).

The series of branches represent various localized states. These states differ from one another by the number of rotating vertical and horizontal junctions. The various states shown in Figs. 8–10 account for different branches in the I_B-V plane in Fig. 11. The lower the branch, the larger is the number M of resistive vertical junctions. The left set of curves accounts for the asymmetric rotobreathers starting at the top with the asymmetric single-site breather and going
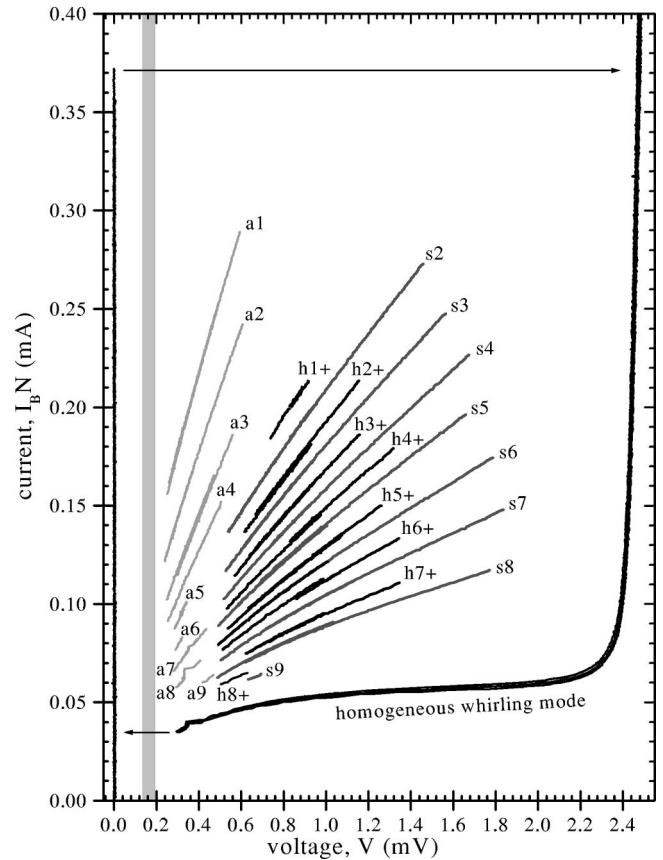
FIG. 11. The I-V characteristic of an annular ladder. The branches correspond to asymmetric ($a\#$), symmetric ($s\#$), and hybrid (coupled) breathers ($h\#+$). The index $\#$ indicates the number of whirling vertical junctions in the main body of the breather.

down to the asymmetric nine-site breather. In Fig. 11 they are marked as $a1$, $a2$, and so on down to $a9$. The curves on the right side correspond to the other localized modes. Counting from the top, the first, the third, and so on are the single-site, two-site, and so on hybrid breathers coupled with a single-site breather, respectively. They are marked in the figure as $h1+$, $h2+$, and so on. For example, the $h3+$ characteristic corresponds to Fig. 10(c) with the three-site hybrid breather. Furthermore, the marks $s2,s3,\ldots$ indicate the symmetric two-site, three-site, $\ldots$ breathers, respectively.

In contrast to the observed characteristics for the linear ladder presented in Fig. 5 all branches in Fig. 11 disappear well below the gap voltage. From the upper end of their traces the symmetric breathers jump to the homogeneous whirling mode, the hybrid-coupled breathers ($h\#$) to the next symmetric breather with higher voltage or a bigger multisite breather or, alternatively, to the homogeneous whirling mode. In most cases, from the upper end of their traces the asymmetric rotobreathers switch to the corresponding symmetric breathers. An exception is the single-site asymmetric breather, which always jumps to the homogeneous whirling mode. Because one edge of the combined breathers has an asymmetric character this state exists in a narrower current range than the symmetric states. Decreasing the bias current I_B leads to another switching behavior. Asymmetric breathers go over to the superconducting state. In most cases, symmet-

ric breathers jump to a higher voltage state.

The instabilities of the observed localized modes may have various reasons. By succeeding the lower end of a characteristic the retrapping current of the horizontal (for symmetric breathers) or all (for asymmetric) junctions is reached. Thus all branches of the symmetric and asymmetric breathers lose their stability at a voltage of about 0.52 mV and 0.28 mV, respectively, which can be seen in Fig. 11. On the upper end of the curves, most probably, the critical current of some adjacent junctions is achieved and the state grows.

Resonances with linear waves are another reason for instabilities. Such resonances have been predicted theoretically [16,17] and already reported in our experiments [10]. Here we observe a few small resonances on the I-V characteristics of the seven- and eight-site asymmetric breathers ($a7$ and $a8$ in Fig. 11). About the voltage at which the resonance occurs the localized modes indicated as $a5$ and $a6$ cease to exist. The resonance voltage agrees fairly well with the double of the upper plasmon band frequency. The plasmon band is identified as a gray region in Fig. 11 for $\gamma = 0.16$.

It is worth noting that waiting for some time (from several seconds to few minutes) at nearly any bias point on a breather characteristic was usually sufficient to lose this particular state. We suppose that this was due to temperature fluctuations and electromagnetic noise of experimental environment.

V. DISCUSSION

Parameter dependences

The region of existence and stability of rotobreathers does sensitively depend on dissipation, discreteness, and anisotropy parameter of the ladder. We studied Josephson junction ladders in a wide parameter range. To give an overview the measured ladders are shown as marks in the η-β_L plane of Fig. 12. Details about other samples investigated can be found elsewhere [18]. The diamonds indicate linear ladders and the circles annular ladders. The open circles point out the previously measured handicapped annular ladders [15]. In all these ladders we found several types of rotobreathers. Increasing the anisotropy factor η makes it more difficult to create breathers. At $\eta = 1$ we found only multisite breathers. We had to retry the creation procedure around a hundred times at this anisotropy until some localized state was catched. The linear ladders with a large self-inductance parameter β_L showed a rather reproducible switching between symmetric and asymmetric breathers. In contrast to that, for the ladders with a small self-inductance this dynamical be-
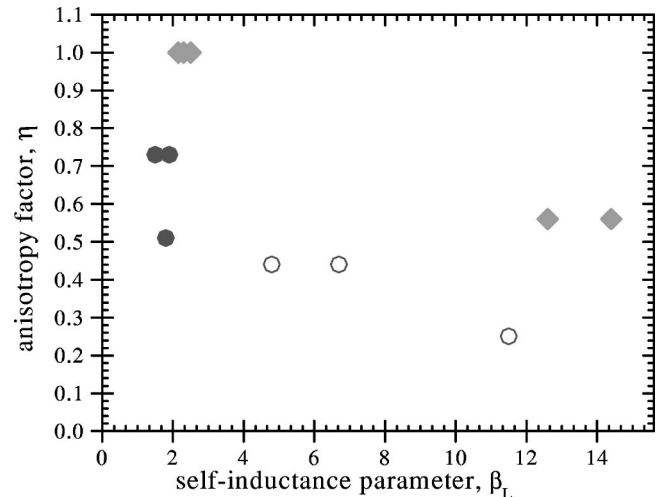
FIG. 12. The anisotropy factor versus the self-inductance parameter of the measured Josephson junction ladders [18]. Diamonds and circles indicate linear and annular ladders, respectively.

havior was more rare to find. It can be argued that larger inductive coupling favors creation of a localized mode. The excitations are also influenced by the damping. At higher temperature and, accordingly, higher damping the localized modes appear seldom. For example, the isotropic ladder at a temperature $T = 6.1$ K ($\alpha \approx 0.13$) showed always truncated six-site breathers during repetitive measurements over several hours; only once in this time an asymmetric four-site breather was found.

In summary, we presented experimental observations of a large variety of spatially localized dynamic states in Josephson ladders with strong coupling. These states were induced by the local current injection and supported by the uniform bias current. We observe many complex states including symmetric, asymmetric, combined, hybrid, coupled, and truncated modes. We stress out that the region of existence and stability of rotobreathers does sensitively depend on dissipation, discreteness, and anisotropy parameter of the ladder.

ACKNOWLEDGMENTS

[1] S. Takeno and M. Peyrard, Physica D **92**, 140 (1996).

[2] S. Aubry, Physica D **103**, 201 (1997).

[3] S. Flach and C. R. Willis, Phys. Rep. **295**, 181 (1998).

[4] B. I. Swanson, J. A. Brozik, S. P. Love, G. F. Strouse, A. P. Shreve, A. R. Bishop, W.-Z. Wang, and M. I. Salkola, Phys. Rev. Lett. **82**, 3288 (1999).

[5] U. T. Schwarz, L. Q. English, and A. J. Sievers, Phys. Rev.

Lett. **83**, 223 (1999).

[6] H. S. Eisenberg, Y. Silberberg, R. Morandotti, A. R. Boyd, and J. S. Aitchison, Phys. Rev. Lett. **81**, 3383 (1998).

[7] E. Trías, J. J. Mazo, and T. P. Orlando, Phys. Rev. Lett. **84**, 741 (2000).

[8] P. Binder, D. Abraimov, A. V. Ustinov, S. Flach, and Y. Zolotaryuk, Phys. Rev. Lett. **84**, 745 (2000).

[9] P. Binder, D. Abraimov, and A. V. Ustinov, Phys. Rev. E **62**, 2858 (2000).

[10] M. Schuster, P. Binder, and A. V. Ustinov, Phys. Rev. E **65**, 016606 (2002).

[11] L. M. Floría, J. L. Marin, P. J. Martinez, F. Falo, and S. Aubry, Europhys. Lett. **36**, 539 (1996).

[12] S. Flach and M. Spicci, J. Phys.: Condens. Matter **11**, 321 (1999).

[13] HYPRES Inc., Elmsford, NY 10523.

[14] A. G. Sivakov, A. P. Zhuravel', O. G. Turutanov, and I. M. Dmitrenko, Appl. Surf. Sci. **106**, 390 (1996).

[15] The data for another type of annular ladders have been reported in Ref. [8]. We have found a specific problem in the layout of this previous type of annular ladders, namely, every second horizontal junction in the inner ring was shorted during fabrication. That explains why mainly breathers with even number of rotating vertical junctions were observed in Ref. [8]. The annular ladder studied in the present paper is free from defects and does not have any shorted junctions.

[16] E. Trías, J. J. Mazo, A. Brinkman, and T. P. Orlando, Physica D **156**, 98 (2001).

[17] A. E. Miroshnichenko, S. Flach, M. V. Fistul, Y. Zolotaryuk, and J. Page, Phys. Rev. E **64**, 066601 (2001).

[18] P. Binder, Ph.D. thesis, Universität Erlangen-Nürnberg, 2002.